

See discussions, stats, and author profiles for this publication at: <https://www.researchgate.net/publication/314246097>

Joint Geometrical and Statistical Alignment for Visual Domain Adaptation

Conference Paper · July 2017

DOI: 10.1109/CVPR.2017.547

CITATIONS

65

READS

463

3 authors:



Jing Zhang

University of Wollongong

16 PUBLICATIONS 524 CITATIONS

SEE PROFILE



Wanqing Li

University of Wollongong

210 PUBLICATIONS 3,548 CITATIONS

SEE PROFILE



Philip O. Ogunbona

University of Wollongong

170 PUBLICATIONS 2,066 CITATIONS

SEE PROFILE

Some of the authors of this publication are also working on these related projects:



Collaborative Watermarking [View project](#)



Action Recognition [View project](#)

Joint Geometrical and Statistical Alignment for Visual Domain Adaptation

Jing Zhang, Wanqing Li, Philip Ogunbona

Advanced Multimedia Research Lab, University of Wollongong, Australia

jz960@uowmail.edu.au, wanqing@uow.edu.au, philipo@uow.edu.au

Abstract

This paper presents a novel unsupervised domain adaptation method for cross-domain visual recognition. We propose a unified framework that reduces the shift between domains both statistically and geometrically, referred to as Joint Geometrical and Statistical Alignment (JGSA). Specifically, we learn two coupled projections that project the source domain and target domain data into low-dimensional subspaces where the geometrical shift and distribution shift are reduced simultaneously. The objective function can be solved efficiently in a closed form. Extensive experiments have verified that the proposed method significantly outperforms several state-of-the-art domain adaptation methods on a synthetic dataset and three different real world cross-domain visual recognition tasks.

1. Introduction

A basic assumption of statistical learning theory is that the training and test data are drawn from the same distribution. Unfortunately, this assumption does not hold in many applications. For example, in visual recognition, the distributions between training and test can be discrepant due to the environment, sensor type, resolution, and view angle. In video based visual recognition, more factors are involved in addition to those in image based visual recognition. For example, in action recognition, the subject, performing style, and performing speed increase the domain shift further. Labelling data is labour intensive and expensive, thus it is impractical to relabel a large amount of data in a new domain. Hence, a realistic strategy, domain adaptation, can be used to employ previous labeled source domain data to boost the task in the new target domain. Based on the availability of target labeled data, domain adaptation can be generally divided into semi-supervised and unsupervised domain adaptation. The semi-supervised approach requires a certain amount of labelled training samples in the target domain and the unsupervised one requires none labelled data. However, in both semi-supervised and unsupervised domain adaptation, sufficient unlabeled target domain data

are required. In this paper, we focus on unsupervised domain adaptation which is considered to be more practical and challenging.

The most commonly used domain adaptation approaches include instance-based adaptation, feature representation adaptation, and classifier-based adaptation [1, 2]. In unsupervised domain adaptation, as there is no labeled data in the target domain, the classifier-based adaptation is not feasible. Alternatively, we can deal with this problem by minimizing distribution divergence between domains as well as the empirical source error [3]. It is generally assumed that the distribution divergence can be compensated either by an instance based adaptation method, such as reweighting samples in the source domain to better match the target domain distribution, or by a feature transformation based method that projects features of two domains into another subspace with small distribution shift. The instance-based approach requires the strict assumptions [1, 4] that 1) the conditional distributions of source and target domain are identical, and 2) certain portion of the data in the source domain can be reused for learning in the target domain through reweighting. While the feature transformation based approach relaxes these assumptions, and only assumes that there exists a common space where the distributions of two domains are similar. This paper follows the feature transformation based approach.

Two main categories of feature transformation methods are identified [5] among the literature, namely data centric methods and subspace centric methods. The data centric methods seek a unified transformation that projects data from two domains into a domain invariant space to reduce the distributional divergence between domains while preserving data properties in original spaces, such as [6, 7, 8, 9]. The data centric methods only exploit shared feature in two domains, which will fail when the two different domains have large discrepancy, because there may not exist such a common space where the distributions of two domains are the same and the data properties are also maximally preserved in the mean time. For the subspace centric methods, the domain shift is reduced by manipulating the subspaces of the two domains such that the sub-

space of each individual domain all contributes to the final mapping [10, 11, 12]. Hence, the domain specific features are exploited. For example, Gong et al. [10] regard two subspaces as two points on Grassmann manifold, and find points on a geodesic path between them as a bridge between source and target subspaces. Fernando et al. [11] align source and target subspaces directly using a linear transformation matrix. However, the subspace centric methods only manipulate on the subspaces of the two domains without explicitly considering the distribution shift between projected data of two domains. The limitations of both data centric and subspace centric methods will be illustrated on a synthetic dataset in Section 4.1.

In this paper, we propose a unified framework that reduces the distributional and geometrical divergence between domains simultaneously by exploiting both the shared and domain specific features. Specifically, we learn two coupled projections to map the source and target data into respective subspaces. After the projections, 1) the variance of target domain data is maximized to preserve the target domain data properties, 2) the discriminative information of source data is preserved to effectively transfer the class information, 3) both the marginal and conditional distribution divergences between source and target domains are minimized to reduce the domain shift statistically, and 4) the divergence of two projections is constrained to be small to reduce domain shift geometrically.

Hence, different from data centric based methods, we do not require the strong assumption that a unified transformation can reduce the distribution shift while preserving the data properties. Different from subspace centric based methods, we not only reduce the shift of subspace geometries but also reduce the distribution shifts of two domains. In addition, our method can be easily extended to a kernelized version to deal with the situations where the shift between domains are nonlinear. The objective function can be solved efficiently in a closed form. The proposed method has been verified through comprehensive experiments on a synthetic dataset and three different real world cross-domain visual recognition tasks: object recognition (Office, Caltech-256), hand-written digit recognition (USPS, MNIST), and RGB-D-based action recognition (MSRAction3DExt, G3D, UTD-MHAD, and MAD).

2. Related Work

2.1. Data centric approach

Pan et al. [6] propose the transfer component analysis (TCA) to learn some transfer components across domains in RKHS using Maximum Mean Discrepancy (MMD) [13]. TCA is a typical data centric approach that finds a unified transformation $\phi(\cdot)$ that projects data from two domains into a new space to reduce the discrepancy. In TCA, the

authors aim to minimize the distance between the sample means of the source and target data in the k -dimensional embeddings while preserving data properties in original spaces. Joint distribution analysis (JDA) [7] improves TCA by considering not only the marginal distribution shift but also the conditional distribution shift using the pseudo labels of target domain. Transfer joint matching (TJM) [8] improves TCA by jointly reweighting the instances and finding the common subspace. Scatter component analysis (SCA) [9] takes the between and within class scatter of source domain into consideration. However, these methods require a strong assumption that there exist a unified transformation to map source and target domains into a shared subspace with small distribution shift.

2.2. Subspace Centric Approach

As mentioned, subspace centric approach can address the issue of data centric methods that only exploit common features of two domains. Fernando et al. [11] proposed a subspace centric method, namely Subspace Alignment (SA). The key idea of SA is to align the source basis vectors (A) with the target one (B) using a transformation matrix M . A and B are obtained by PCA on source and target domains, respectively. Hence, they do not assume that there exist a unified transformation to reduce the domain shifts. However, the variance of projected source domain data will be different from that of target domain after mapping the source subspace using a linear map because of the domain shift. In this case, SA fails to minimize the distributions between domains after aligning the subspaces. In addition, SA cannot deal with situations where the shift between two subspaces are nonlinear. Subspace distribution alignment (SDA) [14] improves SA by considering the variance of the orthogonal principal components. However, the variances are considered based on the aligned subspaces. Hence, only the magnitude of each eigen direction is changed which may still fail when the domain shift is large. This has been validated by the illustration of synthetic data in Figure 2 and the experiment results on real world datasets.

3. Joint Geometrical and Statistical Alignment

This section presents the Joint Geometrical and Statistical Alignment (JGSA) method in detail.

3.1. Problem Definition

We begin with the definitions of terminologies. The source domain data denoted as $X_s \in \mathbb{R}^{D \times n_s}$ are drawn from distribution $P_s(X_s)$ and the target domain data denoted as $X_t \in \mathbb{R}^{D \times n_t}$ are drawn from distribution $P_t(X_t)$, where D is the dimension of the data instance, n_s and n_t are number of samples in source and target domain respectively. We focus on the unsupervised domain adaptation problem. In unsupervised domain adaptation, there are sufficient labeled

source domain data, $\mathcal{D}_s = \{(\mathbf{x}_i, y_i)\}_{i=1}^{n_s}$, $\mathbf{x}_i \in \mathbb{R}^D$, and unlabeled target domain data, $\mathcal{D}_t = \{(\mathbf{x}_j)\}_{j=1}^{n_t}$, $\mathbf{x}_j \in \mathbb{R}^D$, in the training stage. We assume the feature spaces and label spaces between domains are the same: $\mathcal{X}_s = \mathcal{X}_t$ and $\mathcal{Y}_s = \mathcal{Y}_t$. Due to the dataset shift, $P_s(X_s) \neq P_t(X_t)$. Different from previous domain adaptation methods, we do not assume that there exists a unified transformation $\phi(\cdot)$ such that $P_s(\phi(X_s)) = P_t(\phi(X_t))$ and $P_s(Y_s|\phi(X_s)) = P_t(Y_t|\phi(X_s))$, since this assumption becomes invalid when the dataset shift is large.

3.2. Formulation

To address limitations of both data centric and subspace centric methods, the proposed framework (JGSA) reduces the domain divergence both statistically and geometrically by exploiting both shared and domain specific features of two domains. The JGSA is formulated by finding two coupled projections (A for source domain, and B for target domain) to obtain new representations of respective domains, such that 1) the variance of target domain is maximized, 2) the discriminative information of source domain is preserved, 3) the divergence of source and target distributions is small, and 4) the divergence between source and target subspaces is small.

3.2.1 Target Variance Maximization

To avoid projecting features into irrelevant dimensions, we encourage the variances of target domain is maximized in the respective subspaces. Hence, the variance maximization can be achieved as follows

$$\max_B \text{Tr}(B^T S_t B) \quad (1)$$

where

$$S_t = X_t H_t X_t^T \quad (2)$$

is the target domain scatter matrix, $H_t = I_t - \frac{1}{n_t} \mathbf{1}_t \mathbf{1}_t^T$ is the centering matrix, $\mathbf{1}_t \in \mathbb{R}^{n_t}$ is the column vector with all ones.

3.2.2 Source Discriminative Information Preservation

Since the labels in the source domain are available, we can employ the label information to constrain the new representation of source domain data to be discriminative.

$$\max_A \text{Tr}(A^T S_b A) \quad (3)$$

$$\min_A \text{Tr}(A^T S_w A) \quad (4)$$

where S_w is the within class scatter matrix, and S_b is the between class scatter matrix of the source domain data, which are defined as follows,

$$S_w = \sum_{c=1}^C X_s^{(c)} H_s^{(c)} (X_s^{(c)})^T \quad (5)$$

$$S_b = \sum_{c=1}^C n_s^{(c)} (m_s^{(c)} - \bar{m}_s)(m_s^{(c)} - \bar{m}_s)^T \quad (6)$$

where $X_s^{(c)} \in \mathbb{R}^{D \times n_s^{(c)}}$ is the set of source samples belonging to class c , $m_s^{(c)} = \frac{1}{n_s^{(c)}} \sum_{i=1}^{n_s^{(c)}} x_i^{(c)}$, $\bar{m}_s = \frac{1}{n_s} \sum_{i=1}^{n_s} x_i$, $H_s^{(c)} = I_s^{(c)} - \frac{1}{n_s^{(c)}} \mathbf{1}_s^{(c)} (\mathbf{1}_s^{(c)})^T$ is the centering matrix of data within class c , $I_s^{(c)} \in \mathbb{R}^{n_s^{(c)} \times n_s^{(c)}}$ is the identity matrix, $\mathbf{1}_s \in \mathbb{R}^{n_s}$ is the column vector with all ones, $n_s^{(c)}$ is the number of source samples in class c .

3.2.3 Distribution Divergence Minimization

We employ the MMD criteria [13, 6, 7] to compare the distributions between domains, which computes the distance between the sample means of the source and target data in the k-dimensional embeddings,

$$\min_{A,B} \left\| \frac{1}{n_s} \sum_{\mathbf{x}_i \in X_s} A^T \mathbf{x}_i - \frac{1}{n_t} \sum_{\mathbf{x}_j \in X_t} B^T \mathbf{x}_j \right\|_F^2 \quad (7)$$

Long et al. [7] has been proposed to utilize target pseudo labels predicted by source domain classifiers for representing the class-conditional data distributions in the target domain. Then the pseudo labels of target domain are iteratively refined to reduce the difference in conditional distributions between two domains further. We follow their idea to minimize the conditional distribution shift between domains,

$$\min_{A,B} \sum_{c=1}^C \left\| \frac{1}{n_s^{(c)}} \sum_{\mathbf{x}_i \in X_s^{(c)}} A^T \mathbf{x}_i - \frac{1}{n_t^{(c)}} \sum_{\mathbf{x}_j \in X_t^{(c)}} B^T \mathbf{x}_j \right\|_F^2 \quad (8)$$

Hence, by combining the marginal and conditional distribution shift minimization terms, the final distribution divergence minimization term can be rewritten as

$$\min_{A,B} \text{Tr} \left(\begin{bmatrix} A^T & B^T \end{bmatrix} \begin{bmatrix} M_s & M_{st} \\ M_{ts} & M_t \end{bmatrix} \begin{bmatrix} A \\ B \end{bmatrix} \right) \quad (9)$$

where

$$M_s = X_s (L_s + \sum_{c=1}^C L_s^{(c)}) X_s^T, \quad L_s = \frac{1}{n_s^2} \mathbf{1}_s \mathbf{1}_s^T, \quad (10)$$

$$(L_s^{(c)})_{ij} = \begin{cases} \frac{1}{(n_s^{(c)})^2} & \mathbf{x}_i, \mathbf{x}_j \in X_s^{(c)} \\ 0 & \text{otherwise} \end{cases}$$

$$M_t = X_t (L_t + \sum_{c=1}^C L_t^{(c)}) X_t^T, \quad L_t = \frac{1}{n_t^2} \mathbf{1}_t \mathbf{1}_t^T, \quad (11)$$

$$(L_t^{(c)})_{ij} = \begin{cases} \frac{1}{(n_t^{(c)})^2} & \mathbf{x}_i, \mathbf{x}_j \in X_t^{(c)} \\ 0 & \text{otherwise} \end{cases}$$

$$M_{st} = X_s(L_{st} + \sum_{c=1}^C L_{st}^{(c)})X_t^T, \quad L_{st} = -\frac{1}{n_s n_t} \mathbf{1}_s \mathbf{1}_t^T, \quad (12)$$

$$(L_{st}^{(c)})_{ij} = \begin{cases} -\frac{1}{n_s^{(c)} n_t^{(c)}} & \mathbf{x}_i \in X_s^{(c)}, \mathbf{x}_j \in X_t^{(c)} \\ 0 & \text{otherwise} \end{cases}$$

$$M_{ts} = X_t(L_{ts} + \sum_{c=1}^C L_{ts}^{(c)})X_s^T, \quad L_{ts} = -\frac{1}{n_s n_t} \mathbf{1}_t \mathbf{1}_s^T, \quad (13)$$

$$(L_{ts}^{(c)})_{ij} = \begin{cases} -\frac{1}{n_s^{(c)} n_t^{(c)}} & \mathbf{x}_j \in X_s^{(c)}, \mathbf{x}_i \in X_t^{(c)} \\ 0 & \text{otherwise} \end{cases}$$

Note that this is different from TCA and JDA, because we do not use a unified subspace because there may not exist such a common subspace where the distributions of two domains are also similar.

3.2.4 Subspace Divergence Minimization

Similar to SA [11], we also reduce the discrepancy between domains by moving closer the source and target subspaces. As mentioned, an additional transformation matrix M is required to map the source subspace to the target subspace in SA. However, we do not learn an additional matrix to map the two subspaces. Rather, we optimize A and B simultaneously, such that the source class information and the target variance can be preserved, and the two subspaces move closer in the mean time. We use following term to move the two subspaces close:

$$\min_{A, B} \|A - B\|_F^2 \quad (14)$$

By using term (14) together with (9), both shared and domain specific features are exploited such that the two domains are well aligned geometrically and statistically.

3.2.5 Overall Objective Function

We formulate the JGSA method by incorporating the above five quantities ((1), (3), (4), (9), and (14)) as follows:

$$\max \frac{\mu\{\text{Target Var.}\} + \beta\{\text{Between Class Var.}\}}{\{\text{Distribution shift}\} + \lambda\{\text{Subspace shift}\} + \beta\{\text{Within Class Var.}\}}$$

where λ, μ, β are trade-off parameters to balance the importance of each quantity, and Var. indicates variance.

We follow [9] to further impose the constraint that $Tr(B^T B)$ is small to control the scale of B . Specifically, we aim at finding two coupled projections A and B by solving the following optimization function,

$$\max_{A, B} \frac{Tr\left([A^T \quad B^T] \begin{bmatrix} \beta S_b & \mathbf{0} \\ \mathbf{0} & \mu S_t \end{bmatrix} \begin{bmatrix} A \\ B \end{bmatrix}\right)}{Tr\left([A^T \quad B^T] \begin{bmatrix} M_s + \lambda I + \beta S_w & M_{st} - \lambda I \\ M_{ts} - \lambda I & M_t + (\lambda + \mu)I \end{bmatrix} \begin{bmatrix} A \\ B \end{bmatrix}\right)} \quad (15)$$

where $I \in \mathbb{R}^{d \times d}$ is the identity matrix.

Minimizing the denominator of (15) encourages small marginal and conditional distributions shifts, and small within class variance in the source domain. Maximizing the numerator of (15) encourages large target domain variance, and large between class variance in the source domain. Similar to JDA, we also iteratively update the pseudo labels of target domain data using the learned transformations to improve the labelling quality until convergence.

3.3. Optimization

To optimize (15), we rewrite $[A^T \quad B^T]$ as W^T . Then the objective function and corresponding constraints can be rewritten as:

$$\max_W \frac{Tr\left(W^T \begin{bmatrix} \beta S_b & \mathbf{0} \\ \mathbf{0} & \mu S_t \end{bmatrix} W\right)}{Tr\left(W^T \begin{bmatrix} M_s + \lambda I + \beta S_w & M_{st} - \lambda I \\ M_{ts} - \lambda I & M_t + (\lambda + \mu)I \end{bmatrix} W\right)} \quad (16)$$

Note that the objective function is invariant to rescaling of W . Therefore, we rewrite objective function (16) as

$$\max_W Tr\left(W^T \begin{bmatrix} \beta S_b & \mathbf{0} \\ \mathbf{0} & \mu S_t \end{bmatrix} W\right) \quad (17)$$

$$s.t. \quad Tr\left(W^T \begin{bmatrix} M_s + \lambda I + \beta S_w & M_{st} - \lambda I \\ M_{ts} - \lambda I & M_t + (\lambda + \mu)I \end{bmatrix} W\right) = 1$$

The Lagrange function of (17) is

$$L = Tr\left(W^T \begin{bmatrix} \beta S_b & \mathbf{0} \\ \mathbf{0} & \mu S_t \end{bmatrix} W\right) + Tr\left(\left(W^T \begin{bmatrix} M_s + \lambda I + \beta S_w & M_{st} - \lambda I \\ M_{ts} - \lambda I & M_t + (\lambda + \mu)I \end{bmatrix} W - I\right)\Phi\right) \quad (18)$$

By setting the derivative $\frac{\partial L}{\partial W} = 0$, we get:

$$\begin{bmatrix} \beta S_b & \mathbf{0} \\ \mathbf{0} & \mu S_t \end{bmatrix} W = \begin{bmatrix} M_s + \lambda I + \beta S_w & M_{st} - \lambda I \\ M_{ts} - \lambda I & M_t + (\lambda + \mu)I \end{bmatrix} W \Phi \quad (19)$$

where $\Phi = \text{diag}(\lambda_1, \dots, \lambda_k)$ are the k leading eigenvalues and $W = [W_1, \dots, W_k]$ contains the corresponding eigenvectors, which can be solved analytically through generalized eigenvalue decomposition. Once the transformation matrix W is obtained, the subspaces A and B can be obtained easily. The pseudo code of JGSA is summarised in Algorithm 1.

3.4. Kernelization Analysis

The JGSA method can be extended to nonlinear problems in a Reproducing Kernel Hilbert Space (RKHS) using some kernel functions ϕ . We use the Representer Theorem $P = \Phi(X)A$ and $Q = \Phi(X)B$ to kernelize our method, where $X = [X_s, X_t]$ denotes all the source and target training samples, $\Phi(X) = [\phi(x_1), \dots, \phi(x_n)]$ and n is the number of all samples. Hence, the objective function becomes,

Algorithm 1: Joint Geometrical and Statistical Alignment

Input : Data and source labels: X_s, X_t, Y_s ; Parameters: $\lambda = 1, \mu = 1, k, T, \beta$.

Output: Transformation matrices: A and B ; Embeddings: Z_s, Z_t ; Adaptive classifier: f .

- 1 Construct $S_t, S_b, S_w, M_s, M_t, M_{st}$, and M_{ts} according to (2), (3), (4), (10), (11), (12), and (13); Initialize pseudo labels in target domain \hat{Y}_t using a classifier trained on original source domain data;
- 2 **repeat**
- 3 Solve the generalized eigendecomposition problem in Equation (19) and select the k corresponding eigenvectors of k leading eigenvalues as the transformation W , and obtain subspaces A and B ;
- 4 Map the original data to respective subspaces to get the embeddings: $Z_s = A^T X_s, Z_t = B^T X_t$;
- 5 Train a classifier f on $\{Z_s, Y_s\}$ to update pseudo labels in target domain $\hat{Y}_t = f(Z_t)$;
- 6 Update M_s, M_t, M_{st} , and M_{ts} according to (10), (11), (12), and (13).
- 7 **until** Convergence;
- 8 Obtain the final adaptive classifier f on $\{Z_s, Y_s\}$.

$$\max_{P, Q} \frac{\text{Tr}\left([P^T \quad Q^T] \begin{bmatrix} \beta S_b & \mathbf{0} \\ \mathbf{0} & \mu S_t \end{bmatrix} \begin{bmatrix} P \\ Q \end{bmatrix}\right)}{\text{Tr}\left([P^T \quad Q^T] \begin{bmatrix} M_s + \lambda I + \beta S_w & M_{st} - \lambda I \\ M_{ts} - \lambda I & M_t + (\lambda + \mu)I \end{bmatrix} \begin{bmatrix} P \\ Q \end{bmatrix}\right)} \quad (20)$$

where all the X_t 's are replaced by $\Phi(X_t)$ and all the X_s 's are replaced by $\Phi(X_s)$ in $S_t, S_w, S_b, M_s, M_t, M_{st}$, and M_{ts} in the kernelized version.

We replace P and Q with $\Phi(X)A$ and $\Phi(X)B$ and obtain the objective function as follows,

$$\max_{A, B} \frac{\text{Tr}\left([A^T \quad B^T] \begin{bmatrix} \beta S_b & \mathbf{0} \\ \mathbf{0} & \mu S_t \end{bmatrix} \begin{bmatrix} A \\ B \end{bmatrix}\right)}{\text{Tr}\left([A^T \quad B^T] \begin{bmatrix} M_s + \lambda K + \beta S_w & M_{st} - \lambda K \\ M_{ts} - \lambda K & M_t + (\lambda + \mu)K \end{bmatrix} \begin{bmatrix} A \\ B \end{bmatrix}\right)} \quad (21)$$

where $S_t = \tilde{K}_t \tilde{K}_t^T$, $S_w = K_s H_s^{(c)} K_s^T$, with $K = \Phi(X)^T \Phi(X)$, $K_s = \Phi(X)^T \Phi(X_s)$, $K_t = \Phi(X)^T \Phi(X_t)$, $\tilde{K}_t = K_t - \mathbf{1}_t K - K_t \mathbf{1}_n + \mathbf{1}_t K \mathbf{1}_n$, $\mathbf{1}_t \in \mathbb{R}^{n_t \times n}$ and $\mathbf{1}_n \in \mathbb{R}^{n \times n}$ are matrices with all $\frac{1}{n}$. In S_b , $m_s^{(c)} = \frac{1}{n_s^{(c)}} \sum_{i=1}^{n_s^{(c)}} k_i^{(c)}$, $\bar{m}_s = \frac{1}{n_s} \sum_{i=1}^{n_s} k_i$, with $k_i = \Phi(X)^T \phi(x_i)$. In MMD terms, $M_s = K_s(L_s + \sum_{c=1}^C L_s^{(c)})K_s^T$, $M_t = K_t(L_t + \sum_{c=1}^C L_t^{(c)})K_t^T$, $M_{st} = K_s(L_{st} + \sum_{c=1}^C L_{st}^{(c)})K_t^T$, $M_{ts} = K_t(L_{ts} + \sum_{c=1}^C L_{ts}^{(c)})K_s^T$. Once the kernelized objective function (21) is obtained, we can simply solve it in the same way as the original objective function to compute A and B .

4. Experiments

In this section, we first conduct experiments on a synthetic dataset to verify the effectiveness of the JGSA methods. Then we evaluate our method for cross-domain object recognition, cross-domain digit recognition, and cross dataset RGB-D-based action recognition. The codes are available online¹. We compare our method with several state-of-the-art methods: subspace alignment (SA) [11], subspace distribution alignment (SDA) [14], geodesic flow kernel (GFK) [10], transfer component analysis (TCA) [6], joint distribution analysis (JDA) [7], transfer joint matching (TJM) [8], scatter component analysis (SCA) [9], optimal transport (OTGL) [15], and kernel manifold alignment (KEMA) [16]. We use the parameters recommended by the original papers for all the baseline methods. For JGSA, we fix $\lambda = 1, \mu = 1$ in all the experiments, such that the distribution shift, subspace shift, and target variance are treated as equally important. We empirically verified that the fixed parameters can obtained promising results on different types of tasks. Hence, the subspace dimension k , number of iteration T , and regularization parameter β are free parameters.

4.1. Synthetic Data

Here, we aim to synthesize samples of data to demonstrate that our method can keep the domain structures as well as reduce the domain shift. The synthesized source and target domain samples are both draw from a mixture of three RBFian distributions. Each RBFian distribution represents one class. The global means, as well as the means of the third class are shifted between domains. The original data are 3-dimensional. We set the dimensionality of the subspaces to 2 for all the methods.

Figure 2 illustrates the original synthetic dataset and domain adaptation results of different methods on the dataset. It can be seen that after SA method the divergences between domains are still large after aligning the subspaces. Hence, the aligned subspaces are not optimal for reduce the domain shift if the distribution divergence is not considered. The SDA method does not demonstrate obvious improvement over SA, since the variance shift is reduced based upon the aligned subspaces (which may not be optimal) as in SA. TCA method reduces the domain shift effectively. However, two of the classes are mixed up since there may not exist a unified subspace to reduce domain shift and preserve the original information simultaneously. Even with conditional distribution shift reduction (JDA) or instances reweighting (TJM), the class-1 and class-2 still cannot be distinguished. SCA considers the total scatter, domain scatter, and class scatter using a unified mapping. However, there may not exist such a common subspace that satisfies all the constraints.

¹<http://www.uow.edu.au/~jz960/>

Obviously, JGSA aligns the two domains well even though the shift between source and target domains is large.

4.2. Real World Datasets

We evaluate our method on three cross-domain visual recognition tasks: object recognition (Office, Caltech-256), hand-written digit recognition (USPS, MNIST), and RGB-D-based action recognition (MSRAction3DExt, G3D, UTD-MHAD, and MAD). The sample images or video frames are shown in Figure 1.

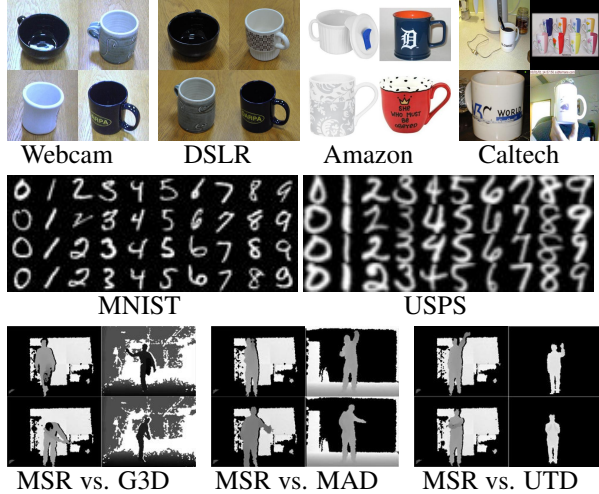


Figure 1: Sample images of object datasets, digit datasets, and sample video frames of depth map of RGB-D-based action datasets.

4.2.1 Setup

Object Recognition We adopt the public Office+Caltech object datasets released by Gong et al. [10]. This dataset contains images from four different domains: Amazon (images downloaded from online merchants), Webcam (low-resolution images by a web camera), DSLR (high-resolution images by a digital SLR camera), and Caltech-256. Amazon, Webcam, and DSLR are three datasets studied in [17] for the effects of domain shift. Caltech-256 [18] contains 256 object classes downloaded from Google images. Ten classes common to four datasets are selected: *backpack, bike, calculator, head-phones, keyboard, laptop, monitor, mouse, mug, and projector*. Two types of features are considered: SURF descriptors (which are encoded with 800-bin histograms with the codebook trained from a subset of Amazon images), and $Decaf_6$ features (which are the activations of the 6th fully connected layer of a convolutional network trained on imageNet). As suggested by [10], 1-Nearest Neighbor Classifier (NN) is chosen as the base classifier. For the free parameters, we set $k = 30$, $T = 10$, and $\beta = 0.1$.

Digit Recognition For cross-domain hand-written digit recognition task, we use MNIST [19] and USPS [20] datasets to evaluate our method. MNIST dataset contains a training set of 60,000 examples, and a test set of 10,000 examples of size 28×28 . USPS dataset consists of 7,291 training images and 2,007 test images of size 16×16 . Ten shared classes of the two datasets are selected. We follow the settings of [7, 8] to construct a pair of cross-domain datasets USPS \rightarrow MNIST by randomly sampling 1,800 images in USPS to form the source data, and randomly sampling 2,000 images in MNIST to form the target data. Then source and target pair are switched to form another dataset MNIST \rightarrow USPS. All images are uniformly rescaled to size 16×16 , and each image is represented by a feature vector encoding the gray-scale pixel values. For the free parameters, we set $k = 100$, $T = 10$, and $\beta = 0.01$.

RGB-D-based Action Recognition For cross-dataset RGB-D-based Action Recognition, four RGB-D-based Action Recognition datasets are selected, namely MSRAction3DExt [21, 22], UTD-MHAD [23], G3D[24], and MAD [25]. All the four datasets are captured by both RGB and depth sensors. We select the shared actions between MSRAction3DExt and other three datasets to form 6 dataset pairs. There are 8 common actions between MSRAction3DExt and G3D: *wave, forward punch, hand clap, forward kick, jogging, tennis swing, tennis serve, and golf swing*. There are 10 common actions between MSRAction3DExt and UTD-MHAD: *wave, hand catch, right arm high throw, draw x, draw circle, two hand front clap, jogging, tennis swing, tennis serve, and pickup and throw*. There are 7 shared actions between MSRAction3DExt and MAD: *wave, forward punch, throw, forward kick, side kick, jogging, and tennis swing forehand*. The local HON4D [26] feature is used for the cross-dataset action recognition tasks. We extract local HON4D descriptors around 15 skeleton joints by following the process similar to [26]. The selected joints include head, neck, left knee, right knee, left elbow, right elbow, left wrist, right wrist, left shoulder, right shoulder, hip, left hip, right hip, left ankle, and right ankle. We use a patch size of $24 \times 24 \times 4$ for depth map with resolution of 320×240 and $48 \times 48 \times 4$ for depth map with resolution of 640×480 , then divide the patches into a $3 \times 3 \times 1$ grid. Since most of the real world applications of action recognition are required to recognize unseen data in the target domain, we further divide the target domain into training and test sets using cross-subject protocol, where half of the subjects are used as training and the rest subjects are used as test when a dataset is evaluated as target domain. Note that the target training set is also unlabeled. For the free parameters, we set $k = 100$ and $\beta = 0.01$. To avoid overfitting to the target training set, we set $T = 1$ in action recognition tasks. LibLINEAR [27] is used for action recognition by following the original paper [26].

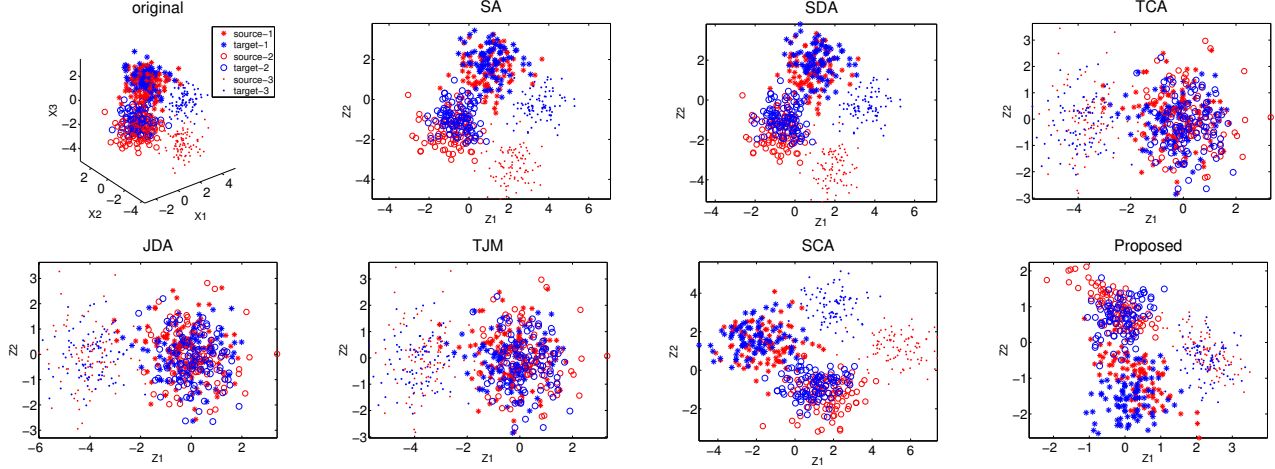


Figure 2: Comparisons of baseline domain adaptation methods and the proposed JGSA method on the synthetic data

Table 1: Accuracy(%) on cross-domain object datasets. Notation for datasets: Caltech:C; Amazon:A; Webcam:W; DSLR:D.

Feature	SURF											Decaf ₆				
data	Raw	SA	SDA	GFK	TCA	JDA	TJM	SCA	JGSA primal	JGSA linear	JGSA RBF	JDA	OTGL	JGSA primal	JGSA linear	JGSA RBF
C→A	36.01	49.27	49.69	46.03	45.82	45.62	46.76	45.62	51.46	52.30	53.13	90.19	92.15	91.44	91.75	91.13
C→W	29.15	40.00	38.98	36.95	31.19	41.69	38.98	40.00	45.42	45.76	48.47	85.42	84.17	86.78	85.08	83.39
C→D	38.22	39.49	40.13	40.76	34.39	45.22	44.59	47.13	45.86	48.41	48.41	85.99	87.25	93.63	92.36	92.36
A→C	34.19	39.98	39.54	40.69	42.39	39.36	39.45	39.72	41.50	38.11	41.50	81.92	85.51	84.86	85.04	84.86
A→W	31.19	33.22	30.85	36.95	36.27	37.97	42.03	34.92	45.76	49.49	45.08	80.68	83.05	81.02	84.75	80.00
A→D	35.67	33.76	33.76	40.13	33.76	39.49	45.22	39.49	47.13	45.86	45.22	81.53	85.00	88.54	85.35	84.71
W→C	28.76	35.17	34.73	24.76	29.39	31.17	30.19	31.08	33.21	32.68	33.57	81.21	81.45	84.95	84.68	84.51
W→A	31.63	39.25	39.25	27.56	28.91	32.78	29.96	29.96	39.87	41.02	40.81	90.71	90.62	90.71	91.44	91.34
W→D	84.71	75.16	75.80	85.35	89.17	89.17	89.17	87.26	90.45	90.45	88.54	100	96.25	100	100	100
D→C	29.56	34.55	35.89	29.30	30.72	31.52	31.43	30.72	29.92	30.19	30.28	80.32	84.11	86.20	85.75	84.77
D→A	28.29	39.87	38.73	28.71	31.00	33.09	32.78	31.63	38.00	36.01	38.73	91.96	92.31	91.96	92.28	91.96
D→W	83.73	76.95	76.95	80.34	86.10	89.49	85.42	84.41	91.86	91.86	93.22	99.32	96.29	99.66	98.64	98.64
Average	40.93	44.72	44.52	43.13	43.26	46.38	46.33	45.16	50.04	50.18	50.58	87.44	88.18	89.98	89.76	88.97

Table 2: Accuracy (%) on cross-domain digit datasets.

data	Raw	SA	SDA	GFK	TCA	JDA	TJM	SCA	JGSA primal
MNIST→USPS	65.94	67.78	65.00	61.22	56.33	67.28	63.28	65.11	80.44
USPS→MNIST	44.70	48.80	35.70	46.45	51.20	59.65	52.25	48.00	68.15
Average	55.32	58.29	50.35	56.84	53.77	63.47	57.77	56.56	74.30

Table 3: Accuracy (%) on cross-dataset RGB-D-based action datasets.

data	Raw	SA	SDA	TCA	JDA	TJM	SCA	JGSA linear
MSR→G3D	72.92	77.08	73.96	68.75	82.29	70.83	70.83	89.58
G3D→MSR	54.47	68.09	67.32	50.58	65.37	63.04	55.25	66.93
MSR→UTD	66.88	73.75	73.75	65.00	77.50	65.00	64.38	76.88
UTD→MSR	62.93	67.91	66.67	57.63	61.06	60.12	55.14	61.37
MSR→MAD	80.71	85.00	83.57	79.29	82.86	82.14	78.57	86.43
MAD→MSR	80.09	81.48	80.56	81.02	83.33	79.63	79.63	85.65
Average	69.67	75.55	74.30	67.05	75.40	70.13	67.30	77.81

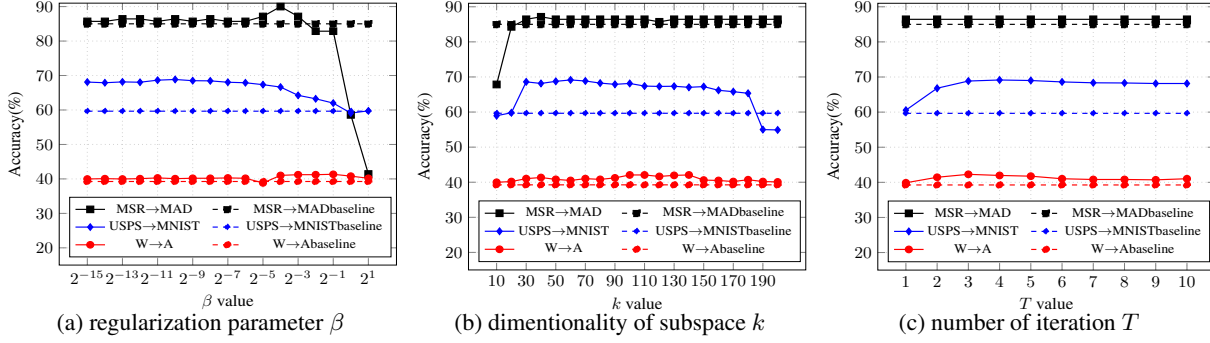


Figure 3: Parameter sensitivity study of JGSA on different types of datasets

4.2.2 Results and Discussion

The results on three types of real world cross domain (object, digit, and action) datasets are shown in Table 1, 2, and 3. The JGSA primal represents the results of JGSA method on original data space, while the JGSA linear and JGSA RBF represent the results with linear kernel and RBF kernel respectively. We follow JDA to report the results on digit datasets in the original feature space. For the action recognition task, it is hard to do eigen decomposition in the original space due to the high dimensionality, hence, the results are obtained using linear kernel. It can be observed that JGSA outperforms the state-of-the-art domain adaptation methods on most of the datasets. As mentioned, the general drawback of subspace centric approach is that the distribution shifts between domains are not explicitly reduced. The data centric methods reduce the distribution shift explicitly. However, a unified transformation may not exist to both reduce distribution shift and preserve the properties of original data. Hence, JGSA outperforms both subspace centric and data centric methods on most of the datasets. We also compare the primal and kernelized versions of the algorithm on the object recognition task (Table 1). The results show that the primal and kernelized versions can obtain similar results on average. To evaluate the effectiveness of pseudo labelling, we compare our method with a semi-supervised method KEMA [16]. We use the same *Decaf7* feature on 8 Office-Caltech dataset pairs as did in KEMA. Our method obtains 90.18% (linear) and 89.91% (RBF), both of which are higher than 89.1% reported in KEMA.

We also evaluated the runtime complexity on the cross-domain object datasets (SURF with linear kernel). The average runtime is 28.97s, which is about three times as long as the best baseline method (JDA). This is because JGSA learns two mappings simultaneously, the size of matrix for eigen decomposition is doubled compared to JDA.

4.2.3 Parameter Sensitivity

We analyse the parameter sensitivity of JGSA on different types of datasets to validate that a wide range of parameter values can be chosen to obtain satisfactory perfor-

mance. The results on different types of datasets have validated that the fixing $\lambda = 1$ and $\mu = 1$ is sufficient for all the three tasks. Hence, we only evaluate other three parameters (k , β , and T). We conduct experiments on the USPS→MNIST, W→A (SURF descriptor with linear kernel), and MSR→MAD datasets for illustration, which are shown in Figure 3. The solid line is the accuracy on JGSA using different parameters, and the dashed line indicates the results obtained by the best baseline method on each dataset. Similar trends are observed on other datasets.

β is the trade-off parameter of within and between class variance of source domain. If β is too small, the class information of source domain is not considered. If β is too big, the classifier would be overfit to the source domain. However, it can be seen from Figure 3a, a large range of β ($\beta \in [2^{-15}, 0.5]$) can be selected to obtain better results than the best baseline method.

Figure 3b illustrates the relationship between various k and the accuracy. We can choose $k \in [20, 180]$ to obtain better results than the best baseline method.

For the number of iteration T , the results on object and digit recognition tasks can be converged to the optimum value after several iteration. However, for the action recognition, the accuracy has no obvious change (Figure 3c). This may be because we use a different protocol for action recognition as mentioned in Section 4.2.1. After iterative labelling (which is done on the target training set), the mappings may be sufficiently good for fitting the target training set, but it is not necessarily the case for the test set.

5. Conclusion

In this paper, we propose a novel framework for unsupervised domain adaptation, referred to as Joint Geometrical and Statistical Alignment (JGSA). JGSA reduces the domain shifts by taking both geometrical and statistical properties of source and target domain data into consideration and exploiting both shared and domain specific features. Comprehensive experiments on synthetic data and three different types of real world visual recognition tasks validate the effectiveness of JGSA compared to several state-of-the-art domain adaptation methods.

References

- [1] S. J. Pan and Q. Yang, "A survey on transfer learning," *IEEE Transactions on Knowledge and Data Engineering*, vol. 22, no. 10, pp. 1345–1359, 2010. [1](#)
- [2] L. Shao, F. Zhu, and X. Li, "Transfer learning for visual categorization: A survey," *IEEE transactions on neural networks and learning systems*, vol. 26, no. 5, pp. 1019–1034, 2015. [1](#)
- [3] S. Ben-David, J. Blitzer, K. Crammer, A. Kulesza, F. Pereira, and J. W. Vaughan, "A theory of learning from different domains," *Machine learning*, vol. 79, no. 1-2, pp. 151–175, 2010. [1](#)
- [4] A. Margolis, "A literature review of domain adaptation with unlabeled data," Tech. Rep., 2011. [1](#)
- [5] Y. Yang and T. Hospedales, "Zero-shot domain adaptation via kernel regression on the grassmannian," in *Proc. the 1st International Workshop on DIFFerential Geometry in Computer Vision for Analysis of Shapes, Images and Trajectories*. BMVA Press, September 2015, pp. 1.1–1.12. [1](#)
- [6] S. J. Pan, I. W. Tsang, J. T. Kwok, and Q. Yang, "Domain adaptation via transfer component analysis," *IEEE Transactions on Neural Networks*, vol. 22, no. 2, pp. 199–210, 2011. [1](#), [2](#), [3](#), [5](#)
- [7] M. Long, J. Wang, G. Ding, J. Sun, and P. Yu, "Transfer feature learning with joint distribution adaptation," in *Proc. IEEE International Conference on Computer Vision*. IEEE, 2013, pp. 2200–2207. [1](#), [2](#), [3](#), [5](#), [6](#)
- [8] M. Long, J. Wang, G. Ding, J. Sun, and P. S. Yu, "Transfer joint matching for unsupervised domain adaptation," in *Proc. IEEE Conference on Computer Vision and Pattern Recognition*. IEEE, 2014, pp. 1410–1417. [1](#), [2](#), [5](#), [6](#)
- [9] M. Ghifary, D. Balduzzi, W. B. Kleijn, and M. Zhang, "Scatter component analysis: A unified framework for domain adaptation and domain generalization," *IEEE Transactions on Pattern Analysis and Machine Intelligence*, vol. PP, no. 99, pp. 1–1, 2016. [1](#), [2](#), [4](#), [5](#)
- [10] B. Gong, Y. Shi, F. Sha, and K. Grauman, "Geodesic flow kernel for unsupervised domain adaptation," in *Proc. IEEE Conference on Computer Vision and Pattern Recognition*, 2012, pp. 2066–2073. [2](#), [5](#), [6](#)
- [11] B. Fernando, A. Habrard, M. Sebban, and T. Tuytelaars, "Unsupervised visual domain adaptation using subspace alignment," in *Proc. IEEE International Conference on Computer Vision*, 2013, pp. 2960–2967. [2](#), [4](#), [5](#)
- [12] B. Fernando, T. Tommasi, and T. Tuytelaars, "Joint cross-domain classification and subspace learning for unsupervised adaptation," *Pattern Recognition Letters*, vol. 65, pp. 60–66, 2015. [2](#)
- [13] A. Gretton, K. M. Borgwardt, M. J. Rasch, B. Schölkopf, and A. Smola, "A kernel two-sample test," *Journal of Machine Learning Research*, vol. 13, pp. 723–773, 2012. [2](#), [3](#)
- [14] B. Sun and K. Saenko, "Subspace distribution alignment for unsupervised domain adaptation," in *Proc. British Machine Vision Conference*, 2015. [2](#), [5](#)
- [15] N. Courty, R. Flamary, D. Tuia, and A. Rakotomamonjy, "Optimal transport for domain adaptation," *IEEE Transactions on Pattern Analysis and Machine Intelligence*, vol. PP, no. 99, pp. 1–1, 2016. [5](#)
- [16] D. Tuia and G. Camps-Valls, "Kernel manifold alignment for domain adaptation," *PloS one*, vol. 11, no. 2, p. e0148655, 2016. [5](#), [8](#)
- [17] K. Saenko, B. Kulis, M. Fritz, and T. Darrell, "Adapting visual category models to new domains," in *European conference on computer vision*. Springer, 2010, pp. 213–226. [6](#)
- [18] G. Griffin, A. Holub, and P. Perona, "Caltech-256 object category dataset," Tech. Rep., 2007. [6](#)
- [19] Y. Lecun, L. Bottou, Y. Bengio, and P. Haffner, "Gradient-based learning applied to document recognition," *Proceedings of the IEEE*, vol. 86, no. 11, pp. 2278–2324, Nov 1998. [6](#)
- [20] J. J. Hull, "A database for handwritten text recognition research," *IEEE Transactions on pattern analysis and machine intelligence*, vol. 16, no. 5, pp. 550–554, 1994. [6](#)
- [21] W. Li, Z. Zhang, and Z. Liu, "Action recognition based on a bag of 3d points," in *Proc. IEEE Computer Society Conference on Computer Vision and Pattern Recognition Workshops*. IEEE, 2010, pp. 9–14. [6](#)
- [22] P. Wang, W. Li, Z. Gao, J. Zhang, C. Tang, and P. O. Ogunbona, "Action recognition from depth maps using deep convolutional neural networks," *IEEE Transactions on Human-Machine Systems*, vol. 46, no. 4, pp. 498–509, Aug 2016. [6](#)
- [23] C. Chen, R. Jafari, and N. Kehtarnavaz, "UTD-MHAD: A multimodal dataset for human action recognition utilizing a depth camera and a wearable inertial sensor," in *Proc. IEEE International Conference on Image Processing*, 2015. [6](#)
- [24] V. Bloom, D. Makris, and V. Argyriou, "G3D: A gaming action dataset and real time action recognition evaluation framework," in *Proc. IEEE Computer Society Conference on Computer Vision and Pattern Recognition Workshops*, June 2012, pp. 7–12. [6](#)
- [25] D. Huang, S. Yao, Y. Wang, and F. De La Torre, "Sequential max-margin event detectors," in *European conference on computer vision*. Springer, 2014, pp. 410–424. [6](#)
- [26] O. Oreifej and Z. Liu, "HON4D: Histogram of oriented 4D normals for activity recognition from depth sequences," in *Proc. IEEE Conference on Computer Vision and Pattern Recognition*. IEEE, 2013, pp. 716–723. [6](#)
- [27] R.-E. Fan, K.-W. Chang, C.-J. Hsieh, X.-R. Wang, and C.-J. Lin, "LIBLINEAR: A library for large linear classification," *Journal of machine learning research*, vol. 9, no. Aug, pp. 1871–1874, 2008. [6](#)